Astronomical Notes

Astronomische Nachrichten

Founded by H. C. Schumacher in 1821

WILEY-VCH

Astron. Nachr. / AN **333**, No. 2, 138 – 152 (2012) / **DOI** 10.1002/asna.201111646

Spot activity on HD 89546 (FG UMa) from long-term photometry*

O. Özdarcan[1,**], **S. Evren**[1], and **G.W. Henry**[2]

[1] Ege University, Faculty of Sciences, Astronomy and Space Sciences Dept., 35100 Bornova - Izmir, Turkey
[2] Center of Excellence in Information Systems, Tennessee State University (TSU), 3500 John A. Merritt Blvd., Box 9501, Nashville, TN 37209, USA

Received 2011 Aug 8, accepted 2012 Jan 13
Published online 2012 Feb 15

Key words binaries: spectroscopic – stars: activity – stars: individual (HD 89546) – stars: rotation – starspots – techniques: photometric

We present the analysis of 20 years of time-series BV photometry of the SB1 RS CVn binary HD 89546. The system's yearly mean V brightness, the $B-V$ color index, the photometric period, and the light curve amplitude all show clear cyclic variability with an ≈9-year time scale. We also find some evidence for brightness variability on a time scale longer than the 20-year time span of our observations, perhaps indicating a longer cycle analogous to the solar Gleissberg cycle. We estimate the unspotted V magnitude of HD 89546 to be $7\overset{m}{.}154$, which is $\approx 0\overset{m}{.}2$ brighter than the observed maximum brightness. Spot modelling of the system shows that spot temperature variations affect the observed $B-V$ color as well as the V brightness. Two active longitudes are observed, centered around 180° and 360° longitude on the G9 III primary, each covering a longitude range of 120°. Furthermore, two inactive longitude zones are seen spanning only 60° between the two active longitudes. The longitudinal distribution of the spots exhibits no strong cyclic variability but does show rapid jumps of 120° that look like the flip-flop phenomenon. We estimate the differential rotation coefficient of the star as $k = 0.086$ by considering the range of observed photometric period variations and assumed latitudinal spot variations over 45°.

1 Introduction

HD 89546 = FG Ursa Majoris is a non-eclipsing SB1 RS CVn binary with a G9 III primary in a circular orbit. The star was initially identified as chromospherically active by W. Bidelman from his objective-prism plates taken at Warner and Swasey Observatory on Kitt Peak (1991, private communication to D. Hall). Strong Ca II H and K emission was reported by Strassmeier (1994) and Strassmeier et al. (1994). Absorption lines of Hα, Hβ and two of the Ca II IRT lines were found to be filled with emission by Henry et al. (1995) and Montes et al. (2000). Henry et al. (1995) made the first photometric observations of HD 89546 and determined a rotation period of $21\overset{d}{.}3$. They also found dramatic variations in the star's amplitude and its mean brightness, typical of strongly active stars. Preliminary analysis of their radial velocity observations indicated a circular orbit with a period of $21\overset{d}{.}5$, suggesting that the binary system is both synchronized and circularized.

Marino et al. (2002) were first to publish an orbital solution for HD 89546, finding a circular orbit with a period of $21\overset{d}{.}37$ and a spectral class of G9-K0 III for the primary component. Fekel et al. (2002) published a more comprehensive spectroscopic and photometric analysis of the star using the first half of the data set presented in this paper. They confirmed the spectral classification of Marino et al. (2002) as G9 III, refined the orbital elements of the system, and estimated the mass of the primary to be 1.0–1.5 $M_\odot$ from its mass function and space motion. They also examined relations between the star's photometric period, yearly mean brightness levels, and light curve amplitude and found a correlation only between mean brightness and amplitude, in the sense that the amplitude got larger as the star got fainter.

In this work, we present a new photometric analysis of HD 89546 with twice the time coverage of Fekel et al. (2002). We investigate cyclic variations in the star and relations between photometric period, light curve amplitude and mean brightness. We estimate a differential rotation coefficient for the G9 III primary from the observed range of photometric periods and an assumed latitudinal spot range. We also apply a spot model to the V data to follow the longitudinal motion of spots on the G9 III component.

2 Observations and data reductions

Most of our Johnson BV photometric observations of HD 89546 were acquired between 1992 March and 2010 May with the Tennessee State University (TSU) T3 0.40 m automatic photoelectric telescope (APT) located at Fairborn Observatory in Southern Arizona. The 0.4 m APT uses a temperature-stabilized EMI 9924B photomultiplier tube to

* Based on data obtained with the Tennessee State University T3 0.4 m APT at Fairborn Observatory, operated by Tennessee State University, and T30 0.3 m telescope of the Ege University Observatory in Izmir.

** Corresponding author: orkun.ozdarcan@ege.edu.tr

acquire data successively through Johnson B and V filters. All observations were made differentially with respect to the comparison star HD 90400 and the check star HD 91480. All of the resulting 2610 differential measurements were corrected for extinction and transformed to the Johnson system with coefficients determined from nightly observations of Johnson standard stars. The typical precision of a single, nightly observation is $\sim$0.004 mag, determined from observations of pairs of constant stars. Further details on the operation and data reduction for the 0.40 m APT can be found in Henry (1995) and Henry et al. (1995).

Additional B and V observations were obtained at Ege University Observatory in 2008 with the 0.30 m Schmidt-Cassegrain telescope (EUO T30) equipped with an SSP-5 photometer. We computed differential magnitudes using the same comparison and check stars as the APT. Details of the data reductions can be found in Özdarcan et al. (2010). The uncertainty of a single EUO observation in the V filter, calculated from the nightly check-minus-comparison star measurements, is $\sim$0.005 mag. We observed photometric standards in the Melotte 111 and Praesepe open clusters on 2009 March 27 and April 17 to determine transformation coefficients for T30 and to derive apparent magnitudes for the comparison and check stars. Transformation equations for the EUO observations can be found in the appendix (Eqs. (A1) and (A2)). Finally, all transformed T3 and T30 differential magnitudes were converted to apparent magnitudes with $V = 6\overset{\mathrm{m}}{.}888$ and $B - V = 1\overset{\mathrm{m}}{.}041$ for HD 90400 and $V = 5\overset{\mathrm{m}}{.}173$ and $B - V = 0\overset{\mathrm{m}}{.}336$ for HD 91480.

3 Interstellar reddening and astrophysical parameters

Multicolor UBV observations of an active star at its unspotted brightness level allow it to be plotted on a color-color diagram and to determine the level of interstellar reddening and its effect on the star's measured astrophysical properties. Unfortunately, only the $B - V$ color index is available for HD 89546. However, given the star's high galactic latitude ($b = 48°$) and its Hipparcos parallax of 5.29 ± 0.70 mas (van Leeuwen 2007), interstellar reddening should be negligible for HD 89546. Therefore, we used the unspotted V magnitude and $B - V$ color index (determined in the next section) to make estimates of the star's effective temperature to be 4720 K (with the calibration of Drilling & Landolt 2000), 4920 K (with the calibration of Flower (1996) and 4970 K (from Gray (2005). For the current analysis, we adopt the calibration of Flower (1996) and take the effective temperature to be $4920 \ \pm \ 100$ K.

We adopt the $v \sin i$ value of 18 ± 1 km s^{-1} of Fekel et al. (2002) and estimate the stellar radius from the Stefan-Boltzmann law and the unspotted V magnitude of the star (solar $M_{\rm bol} = 4\overset{\mathrm{m}}{.}74$). The resulting inclination is $i \approx 50°$ which agrees well with the value of $i \approx 57°$ from Fekel et al. (2002). We believe that the real uncertainty in the inclination is larger due to the large uncertainties in radii of giant stars. We list the astrophysical parameters HD 89546 in Table 1.

Table 1 Absolute photometric parameters of HD 89546. The bolometric correction, BC, was taken from Flower (1996).

Parameter	Value
V_0	$7\overset{\mathrm{m}}{.}154$
$E(B-V)$ (assumed)	$0\overset{\mathrm{m}}{.}0$
$(B-V)_0$	$0\overset{\mathrm{m}}{.}96$
$T_{\rm eff}$ (K)	4920 ± 100
BC	–0.342
Hipparcos distance (pc)	189^{+29}_{-22}
M_V	$0\overset{\mathrm{m}}{.}77 \pm 0\overset{\mathrm{m}}{.}35$
$M_{\rm bol}$	$0\overset{\mathrm{m}}{.}42$
$v \sin i$ (km s^{-1})	18 ± 1
Inclination (deg)	$49 \pm$
Radius ($R_\odot$)	10.0 ± 0.7
Luminosity ($L_\odot$)	53 ± 6

4 Mean brightness, color, amplitude, and unspotted brightness

We plot our 20-yr time series of V magnitudes and $B - V$ color indices of HD 89546 in Fig. 1. Each cluster of points represents one of the 20 observing seasons, which last typically from early November to mid June of the following year. The most obvious features of the light and color curves are the dramatic variations in mean V brightness from year to year accompanied by smaller but in phase variations in the seasonal mean $B - V$ color index. These correlated changes are in the sense that the star becomes redder as it becomes fainter and *vice versa*. The seasonal mean brightness varies over a wide range of $\sim 0\overset{\mathrm{m}}{.}35$, while the seasonal mean color indices vary over a much smaller range of $\sim 0\overset{\mathrm{m}}{.}04$. This is indicative of cool, dark spots on the surface of HD 89546 as the dominant activity structures.

Furthermore, when we consider the rotational amplitudes of the $B - V$ color index within individual observing seasons, we find them to fall in the range $0\overset{\mathrm{m}}{.}015 - 0\overset{\mathrm{m}}{.}025$, similar to the $0\overset{\mathrm{m}}{.}04$ range we see in the seasonal means. This similarity between the rotational amplitude and the range of the seasonal means implies that these variations come primarily from the same source, namely variations in spot temperatures. We will perform quantitative modelling of spot temperatures in Sect. 8.

In addition to the correlated changes in seasonal mean brightness and mean color index, Fig. 1 shows that complex changes in the brightness, amplitude, and light curve shape also occur *within* individual observing seasons. The night-to-night changes in stellar brightness and color index are interpreted as rotational modulation in the visibility of spot regions. The longer year-to-year variations in the mean light level and shape of the light curve are the result of changes in the total level and continual redistribution of spottedness on

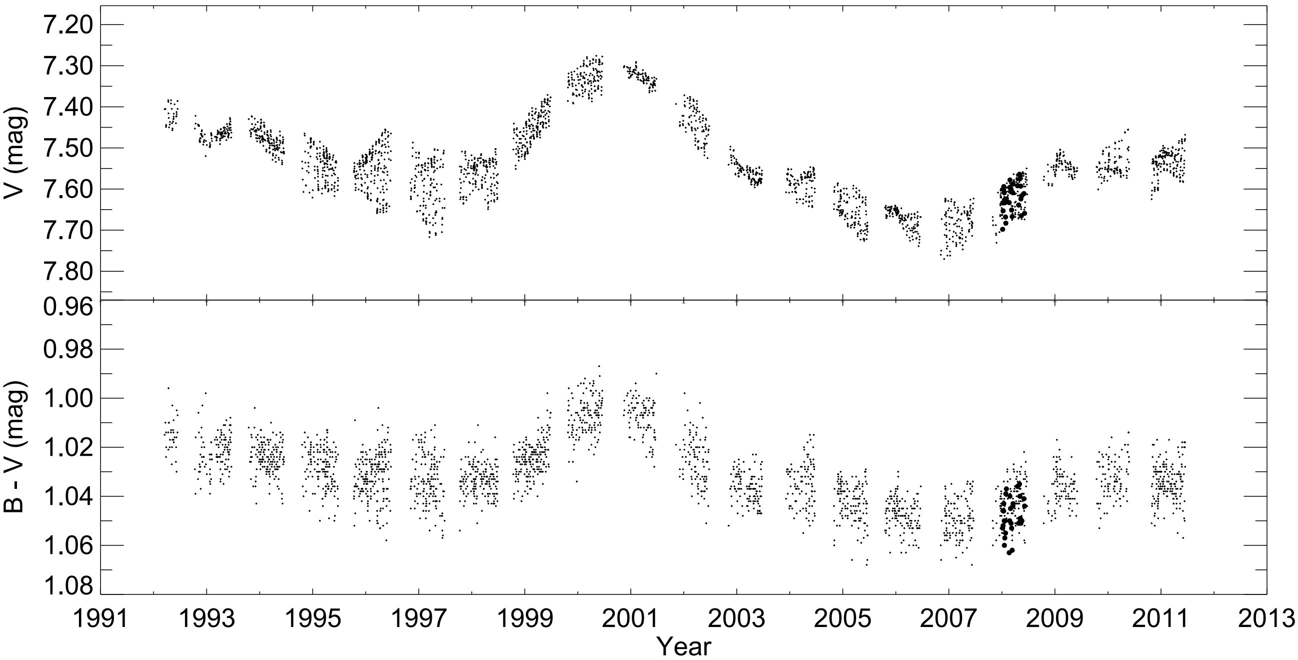

Fig. 1 Twenty years of V (*upper panel*) and $B - V$ (*lower panel*) photometry of HD 89546. Small dots denote data from the TSU 0.40 m APT while filled circles in 2008 represent data from T30 at EUO. Bright ends of the y axes of both panels correspond to estimated unspotted brightness and color index values. See Sect. 4 for details.

the stellar surface via differential rotation and/or the growth and decay of spot regions at various locations on the star (see, e.g., Henry et al. 1995).

In preparation for light curve analysis, we divide our 20 year time series of V and $B - V$ observations into 54 subsets, each chosen to minimize changes in the light curve within each subset. For each subset, we use the maximum and minimum brightness levels to determine the amplitude and mean brightness of the light curve, computed as their difference and mean, respectively. The results for all 54 subsets are tabulated in Table 2. In Fig. 2, we plot the minimum (top), maximum (middle), and mean magnitudes (bottom) vs. amplitude for all 54 subsets.

The top panel of Fig. 2 exhibits only modest correlation of the light curve amplitude with the seasonal minimum brightness of HD 89546. As can be seen clearly in Fig. 1, low-amplitude brightness variations of HD 89546 can be seen both when the star is bright and when it is faint. However, we can use the top panel of Fig. 2 to estimate the star's unspotted brightness level using the method of Oláh et al. (1997). We fit a straight line to the upper envelope of the distribution (plotted as open squares in the top panel) and extend it until it intersects the vertical axis. The resulting unspotted brightness level is $7\overset{\mathrm{m}}{.}154$. Application of this same method to our B data gives $8\overset{\mathrm{m}}{.}114$ as the unspotted brightness level in the B band. The difference between these two values gives us the unspotted $B - V$ color index of $0\overset{\mathrm{m}}{.}96$. The unspotted brightness in the V band is considerably brighter ($0\overset{\mathrm{m}}{.}2$) than the observed brightness maximum seen in 2001. That difference, together with the dramatic variations in mean brightness and amplitude throughout the

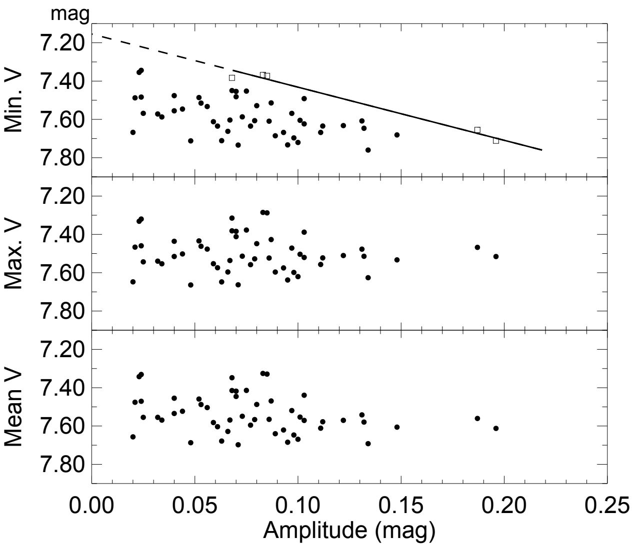

Fig. 2 Minimum (top), maximum ($middle$), and mean ($bottom$) brightness of HD 89546 vs. amplitude.

20-year timespan of our observations, indicates a very high level of activity in HD 89546.

The bottom panel of Fig. 2 shows there is little correlation between the amplitude and seasonal mean brightness, i.e., similar amplitudes can occur across a range of seasonal mean brightness levels. Only for the largest amplitudes do we see a slight tendency toward lower mean magnitudes. Fekel et al. (2002) found a somewhat stronger correlation between amplitude and mean brightness, but this has weakened here with a doubling of the time coverage.

Table 2 Basic properties of the 54 photometric subsets.

Set Number	Start-End Dates (HJD − 2 400 000)	Time Span (days)	$N_{\rm obs}$	Max. V (mag)	Min. V (mag)	Mean V (mag)	Amplitude (mag)
1	48696.78 – 48785.65	89	30	7.382	7.450	7.416	0.068
2	48906.02 – 48988.95	83	26	7.467	7.488	7.477	0.021
3	49044.90 – 49115.70	71	40	7.460	7.484	7.472	0.023
4	49117.70 – 49156.65	39	27	7.436	7.476	7.456	0.040
5	49277.00 – 49393.87	117	68	7.434	7.486	7.460	0.052
6	49398.82 – 49436.71	38	32	7.463	7.515	7.489	0.052
7	49439.84 – 49519.65	80	52	7.477	7.533	7.505	0.056
8	49644.99 – 49734.05	89	38	7.478	7.608	7.543	0.131
9	49744.98 – 49820.82	76	76	7.504	7.605	7.554	0.101
10	49821.83 – 49891.65	70	41	7.523	7.609	7.566	0.086
11	50001.01 – 50074.88	74	45	7.536	7.603	7.570	0.067
12	50077.85 – 50122.80	45	49	7.520	7.623	7.572	0.103
13	50123.83 – 50256.65	133	114	7.468	7.655	7.562	0.187
14	50392.01 – 50459.98	68	32	7.515	7.646	7.580	0.132
15	50465.83 – 50518.79	53	45	7.533	7.681	7.607	0.148
16	50520.81 – 50625.65	105	75	7.515	7.712	7.613	0.196
17	50731.02 – 50782.95	52	28	7.510	7.632	7.571	0.122
18	50787.03 – 50900.78	114	72	7.528	7.607	7.567	0.079
19	50903.80 – 50992.65	89	65	7.523	7.635	7.579	0.112
20	51099.01 – 51201.87	103	67	7.448	7.528	7.488	0.080
21	51206.97 – 51282.74	76	66	7.412	7.482	7.447	0.070
22	51283.74 – 51355.66	72	52	7.384	7.454	7.419	0.070
23	51476.02 – 51578.00	102	43	7.315	7.383	7.349	0.068
24	51578.91 – 51640.83	62	42	7.287	7.373	7.330	0.085
25	51644.79 – 51712.65	68	49	7.285	7.368	7.327	0.083
26	51975.81 – 52031.72	56	27	7.320	7.344	7.332	0.024
27	52034.73 – 52084.66	50	28	7.332	7.355	7.343	0.023
28	52221.01 – 52348.85	128	42	7.378	7.452	7.415	0.075
29	52349.85 – 52380.76	31	22	7.389	7.492	7.440	0.103
30	52384.73 – 52447.67	63	35	7.427	7.514	7.470	0.087
31	52583.02 – 52728.82	146	63	7.525	7.565	7.545	0.040
32	52730.81 – 52811.66	81	54	7.553	7.587	7.570	0.034
33	52978.03 – 53023.97	46	20	7.554	7.612	7.583	0.059
34	53034.00 – 53095.89	62	27	7.574	7.635	7.605	0.061
35	53101.77 – 53176.67	75	56	7.558	7.635	7.596	0.077
36	53308.99 – 53393.89	85	51	7.596	7.662	7.629	0.066
37	53395.83 – 53464.79	69	35	7.599	7.697	7.648	0.098
38	53470.72 – 53539.68	69	46	7.620	7.720	7.670	0.100
39	53660.00 – 53753.93	94	63	7.647	7.668	7.657	0.020
40	53757.94 – 53841.72	84	38	7.664	7.712	7.688	0.048
41	53842.72 – 53905.67	63	31	7.663	7.734	7.699	0.071
42	54045.01 – 54117.95	73	38	7.626	7.760	7.693	0.134
43	54125.00 – 54194.76	70	40	7.638	7.733	7.686	0.095
44	54204.72 – 54268.68	64	36	7.648	7.711	7.680	0.063
45	54402.01 – 54507.86	106	56	7.597	7.686	7.641	0.089
46	54520.86 – 54584.72	64	54	7.575	7.668	7.622	0.093
47	54586.72 – 54638.67	52	36	7.557	7.668	7.612	0.111
48	54838.95 – 54906.85	68	46	7.516	7.555	7.536	0.040
49	54914.78 – 54983.71	69	29	7.543	7.568	7.556	0.025
50	55117.01 – 55213.91	97	43	7.514	7.587	7.550	0.073
51	55221.87 – 55339.70	118	55	7.472	7.569	7.520	0.097
52	55497.01 – 55550.02	53	49	7.527	7.603	7.565	0.076
53	55554.92 – 55658.81	104	77	7.506	7.559	7.533	0.054
54	55662.74 – 55726.66	64	47	7.484	7.582	7.533	0.098

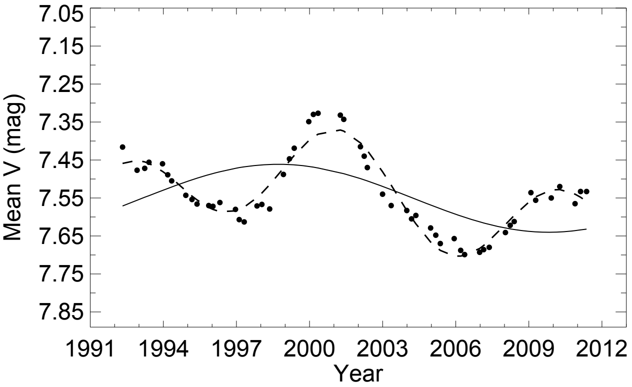

Fig. 3 Mean V brightness variation over 20 years (filled circles). The solid curve represents the possible ≈22-yr period while dashed curve shows the combination of the 22-yr and 9-yr cycles.

5 Mean brightness variation and spot cycle

Long-term brightness variations in objectHD 89546, as seen in the mean V magnitudes plotted in Fig. 3, suggest a cyclic variation similar to the variation in the Sun's total irradiance during its 11-yr Schwabe cycle. Two light minima and one light maximum are seen in Fig. 3, with the second minimum (around 2006) deeper by $0\overset{m}{.}1$ than the first minimum (around 1997). This may indicate a second, longer brightness cycle in HD 89546. We investigate these brightness variations by applying standard Fourier analysis with Period04 software (Lenz & Breger 2005). The analysis indicates a ≈9-yr cycle and suggests longer-term variability on the time scale of the current data set (≈22 yr). We represent these cycles in Fig. 3 with smooth curves.

Since the rotational period of HD 89546 is synchronized with its orbital period, we can plot the 9-yr and 22-yr cycles in the orbital period vs. cycle length diagram of Fig. 4, taken from Oláh & Strassmeier (2002). Three linear trends in the diagram show the changing lengths of short-, medium- and long-term activity cycles with rotation period, from bottom to top, respectively. We over plot the 9-yr period (with an open 4-point star) and see that it nicely fits the observed trend for short-term cycles. We also plot the 22-yr period (a filled 4-point star) in the diagram and we see that it agrees with the trend for medium-term cycles. The existence of a 22-yr cycle is inconclusive, however, and needs more photometric monitoring to confirm. We assume, however, that the 22-yr cycle is real and is related to the magnetic activity of the star. Therefore, we remove the 22-yr variation from the photometric time series and perform our further analysis on the pre-whitened observations. Here, our aim is to remove the effects of a symmetric activity component (22-yr variation), such as a polar cap, a spot strip around the star, or background spottedness, since these do not result in rotational modulation in the star's brightness. Removing these effects is a more consistent way to investigate the rotational modulation.

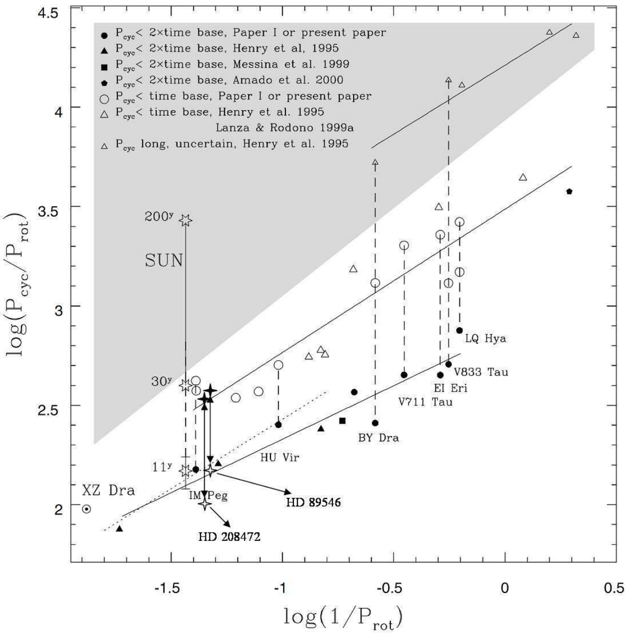

Fig. 4 Relation between rotation period and activity cycle lengths. The figure is taken from Oláh & Strassmeier (2002). Observed cycle periods of HD 89546 are over plotted with empty and filled 4-point stars and connected to each other. We also plot cycle lengths of HD 208472 (Özdarcan et al. 2010) in the same way.

6 Photometric period variation and differential rotation

Since the 54 photometric subsets have relatively few observations, it is not possible to calculate accurate photometric periods for each subset. Instead, we divide our whole pre-whitened V dataset into 20 subsets to determine a mean photometric period for each observing season. We also determine mean amplitude and brightness values for each observing season. For asymmetric or double-humped light curves in spotted stars, it's better to use statistical methods to determine accurate photometric periods. Here, we adopt the ANOVA method (Schwarzenberg-Czerny 1996) and use the PERANSO software (Vanmunster 2007) to apply the method. We list the resulting periods, mean brightness, and amplitudes in Table 3. The photometric periods are plotted Fig. 5, together with the pre-whitened mean brightnesses and light curve amplitudes. The photometric periods tend to be shorter than the orbital period.

In Fig. 5, one can see that the photometric period decreases during the 9-yr interval from 1993 to 2002 (first group), as shown with the straight line segment. During the same interval, the mean brightness first decreases and then increases while the amplitude first increases and then decreases. Similar variations are seen during the 7-yr interval from 2003 to 2010 (second group). The similar time scales of these variations supports our interpretation of a 9-yr cycle.

In the first group, the range of photometric periods is 0.9 day, while in the second group is 0.4 day. The two different

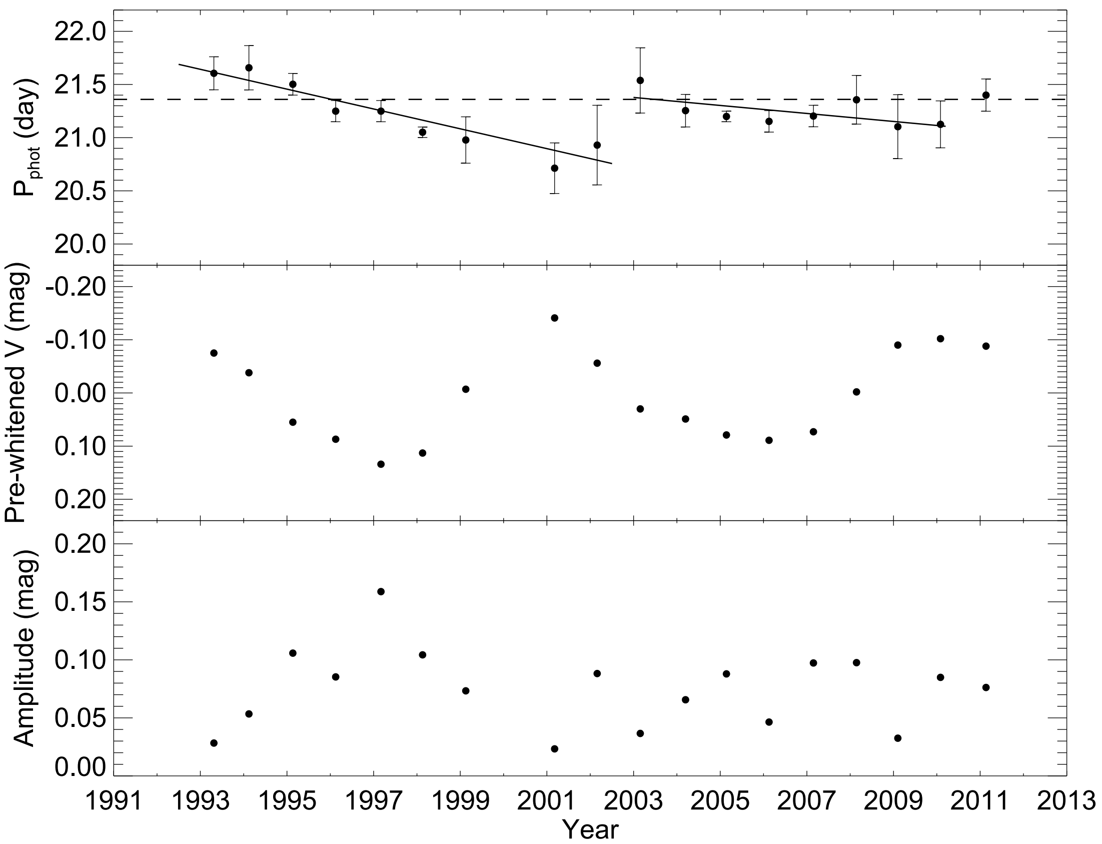

Fig. 5 Photometric periods, pre-whitened brightness and V light curve amplitudes of HD 89546 over time (*from top to bottom*). Horizontal dashed line in the upper panel gives the orbital period, while the solid lines represent the trend in photometric periods (see text).

period ranges indicate that the photometric period is not directly affected by differential rotation. Growth and decay of spot regions at different latitudes and longitudes may result in photometric period variations (Fekel et al. 2002). On the other hand, the photometric period depends on the size and age of spots, their structure (spot or spot groups) and their connection inside the convective zone (Pulkkinen & Tuominen 1998; Hathaway & Wilson 1990). Since we see similarities in the time scale of variability of the period, amplitude, and brightness, we believe that differential rotation is an important source of the period variation.

In principle, one can estimate spot latitudes from photometric spot modelling and use the photometric periods and latitudes to estimate the differential rotation coefficient, k. However, determination of spot latitudes from photometry is an ill-posed problem. Another approach for estimating k is to take the range of the seasonal photometric periods and assume a latitude range for the corresponding spot regions. Following the latter method, we make use of the relations given by Hall & Busby (1990),

$$\frac{P_{\max} - P_{\min}}{P_{\rm eq}} = kf, \tag{1}$$

where

$$f = \sin^2\theta_{\max} - \sin^2\theta_{\min}, \tag{2}$$

and $P_{\max}$ and $P_{\min}$ are the longest and the shortest observed photometric period, respectively, and θ denotes spot latitude. If we adopt a solar analogy, then we can take $P_{\rm eq} = P_{\min}$ and use a solar-type differential rotation law for HD 89546. Hall & Busby (1990) give f values between 0.5 and 0.7 for a latitude range of 45°, depending on whether the spots are near equatorial, intermediate, or polar latitudes. Finally, k can be estimated from the adopted value of f.

The photometric periods from sets #2 and #10 are the longest ($P = 21\overset{\rm d}{.}605$) and shortest ($P = 20\overset{\rm d}{.}709$) periods, respectively. We assume the shortest period is the equatorial rotation period. This gives $k = 0.086$ for $f = 0.5$ and $k = 0.062$ for $f = 0.7$. Now we can estimate spot latitudes from the photometric periods using another relation from by Hall & Busby (1990),

$$P_\theta = \frac{P_{\rm equ}}{(1 - k\sin^2\theta)}. \tag{3}$$

From $P_{\max}$ and $P_{\min}$ from observing seasons #2 and #10, we compute a latitude range of 55° for $k = 0.062$ and 44° for $k = 0.086$. Since we have assumed a 45° latitude range, we take $f = 0.5$ and $k = 0.086$ as our best estimation of the differential rotation coefficient. Implicit in this estimate is the assumption that the primary cause of the period variation is differential rotation, uncomplimented by

Table 3 Numerical values for the seasonal photometric periods, mean V brightness, and V light curve amplitudes, mean V brightnesses residuals, and calculated spot latitudes θ in degrees (see text).

Set	Year	Period (day)	Mean V (mag)	Ampl. (mag)	Residual (mag)	θ (°)
1	1992.33	21.199 ± 0.200	7.415	0.068	–0.152	31
2	1993.31	21.605 ± 0.155	7.467	0.028	–0.075	44
3	1994.12	21.604 ± 0.208	7.484	0.053	–0.038	44
4	1995.14	21.511 ± 0.102	7.553	0.106	0.055	41
5	1996.12	21.305 ± 0.100	7.567	0.085	0.087	35
6	1997.17	21.254 ± 0.100	7.599	0.159	0.134	33
7	1998.13	21.053 ± 0.049	7.571	0.104	0.113	26
8	1999.13	20.905 ± 0.218	7.450	0.073	–0.007	19
9	2000.14	21.203 ± 0.100	7.334	0.068	–0.130	31
10	2001.18	20.709 ± 0.238	7.337	0.023	–0.141	5
11	2002.16	20.931 ± 0.374	7.441	0.088	–0.056	20
12	2003.15	21.538 ± 0.307	7.549	0.037	0.030	42
13	2004.20	21.254 ± 0.153	7.594	0.066	0.049	33
14	2005.14	21.199 ± 0.050	7.648	0.088	0.079	31
15	2006.13	21.153 ± 0.101	7.680	0.046	0.089	29
16	2007.15	21.203 ± 0.101	7.685	0.097	0.073	31
17	2008.15	21.356 ± 0.229	7.624	0.098	–0.002	36
18	2009.10	21.103 ± 0.301	7.545	0.033	–0.090	28
19	2010.08	21.125 ± 0.221	7.534	0.085	–0.102	28
20	2011.14	21.400 ± 0.152	7.542	0.076	–0.088	38

the effects of spot region growth and decay. Clearly, the sign of k needs to be confirmed. With a $v \sin i$ value of $18\,\mathrm{km\,s^{-1}}$, HD 89546 is a good candidate for Doppler imaging.

From the assumption that $k = 0.086$, we can compute spot latitudes for each of the 20 observing seasons. We have listed the spot latitudes in Table 3. If the orbital period is the rotation period of the co-rotation latitude on the star, then, under the assumption of solar-type differential rotation, we use the relations above to calculate a co-rotation latitude of 36°. The uncertainties in the latitudes in Table 3 can be estimated from the uncertainties of the photometric periods and are usually around 7°.

7 Photometric period-amplitude-brightness relations

The Maximum brightness of the HD 89546 system reached a maximum in 2001 while the photometric period and amplitude were near their minimum values. We take this year to be the end of first cycle (1993–2001) and the beginning of the second cycle, though we believe there was some overlap in the two cycles. The second cycle began around 2003 and seems close to finish by 2011 data, where pre-whitened brightness reaches its local maximum, photometric period increases and amplitude starts to decrease. Our ~9-yr cycle length, determined from the 54 subsets of the prewhitened data, is in good agreement with the time scales of the seasonal mean periods, V brightness, and amplitudes.

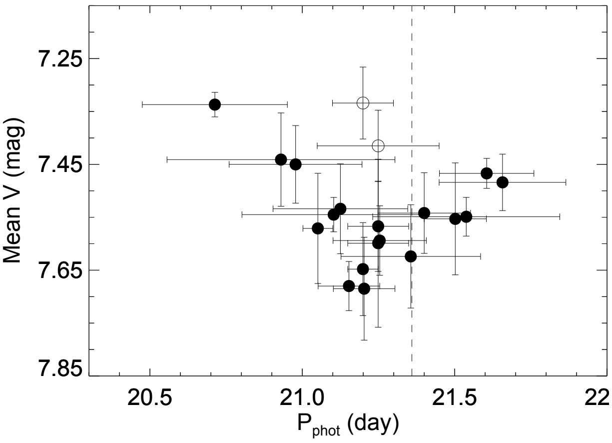

Fig. 6 Photometric period-mean V brightness diagram. Vertical dashed line represents orbital period. See text for the explanation of two empty circles.

When the pre-whitened seasonal mean brightness is at a minimum in 1997 (see Fig. 5), the photometric period is close to the orbital period, and the light curve amplitude reaches a local maximum. In the second cycle, the amplitudes in 2006 and 2009 are small relative to the neighbouring years. If these two data points are not considered, then we can still see that amplitudes reach local maximum value with decreasing brightness and vice-versa. The smaller amplitudes in 2006 and 2009 likely the result of spot re-distribution on the surface of the star. Similarly, spot redistribution to opposite hemispheres of the star, together with increasing activity level, likely resulted in the large amplitude in 1997.

In Fig. 6, we compare the photometric periods and mean V brightness levels for the 20 individual observing seasons. Horizontal error bars indicate the uncertainty in the period determination; vertical bars show the seasonal mean amplitude (see Table 3). One can see an increasing trend in mean brightness with decreasing periods when the photometric periods are shorter than the orbital period. For rotation periods longer than the orbital period, we again see an increasing trend in mean brightness but with *increasing* period. There is a V-shape to the lower envelope of the distribution that is similar to the sunspot cycle pattern in terms of mean brightness and photometric period. At the beginning of a spot cycle, mean brightness is at maximum (minimal spot coverage) and the photometric period is longest. In the middle of the cycle, mean brightness is at minimum (maximum spot coverage) and the photometric period is intermediate between its maximum and minimum values. At the end of cycle mean brightness is again at maximum and photometric period returns to its longest. There are some measurements that do not adhere strictly to this pattern. The two data points that are shown as open circles in Fig. 6 show that the star was brighter at those times relative to the fading trend in mean V brightness. Those points belong to data

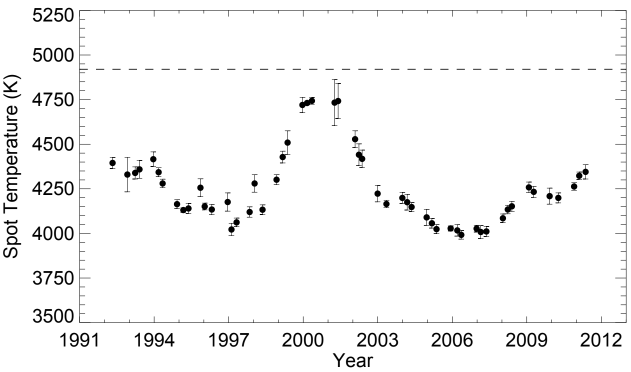

Fig. 7 Calculated spot temperatures from $B - V$ color indices over time for the 54 subsets of our photometric time series. The horizontal dashed line shows our estimated effective temperature of the unspotted photosphere.

sets #1 and #9 and those times are very close to maximum V brightness. In the context of our cycle interpretation, maximum light corresponds to the end of one cycle and the beginning of the next. There may be some overlapping of the two cycles, so we might expect to see some variation from the general trend of the spot cycle, but Fig. 6 suggests a relation between the mean brightness and the photometric period.

8 Spot modelling

The light curves of HD 89546 are usually asymmetric or double humped, which indicates the need to model two separate spots (or spot groups). For our spot modelling we use the SpotModel code (Ribárik et al. 2003) to apply Budding's model (1977) for two spots. The code uses the Marquardt-Levenberg non-linear least squares fitting algorithm (Levenberg 1944; Marquardt 1963). Due to the continuous changes of our HD 89546 light curves, we model the same 54 subsets listed in Table 2 and used to determine the light curve maxima, minima, means, and amplitudes. However, for the spot modelling, we use the pre-whitened data with the $\sim$22-yr removed.

We fix several parameters before the modelling process. First of all, we fixed inclination of rotational axis and passband – dependent linear limb darkening coefficients from van Hamme (1993). We mentioned that variation in $B - V$ must come from variation in spot temperatures, therefore we can use color indices of every individual subset to determine and fix the spot temperatures. SpotModel code has ability to calculate spot temperatures from two color data. We calculate spot temperature for every individual data set. In Fig. 7 we show resulting spot temperatures.

Spot temperatures are not constant throughout the years. Furthermore, spot temperatures exhibit the same variation behaviour with $B - V$ color indices, i.e. when the color gets redder, spot temperatures get decrease and vice-versa (see Fig. 1 lower panel and Fig. 7). Mean brightness varies in the same way with $B - V$ color, i.e. when the brightness is minimum, the color is redder and vice-versa. Those relations imply that 8.86-yr variation in mean brightness must be related to spot temperature variation.

After spot temperature determination, we can fix flux ratio between spot and unspotted photosphere for each subset. We calculated spot latitudes in previous section for 20 observing seasons. Here, we assume that photometric period is constant during every individual season so the spot latitude is. When considering the 54 subsets, we assume the same latitude value for different subsets in the same observing season. Therefore, remaining unknown parameters are radii and longitudes of spots. For every subsets, we assume its local maximum light level as unspotted brightness, because we can not resolve the source of global mean brightness variation which indicates symmetric component of activity (growing-shrinking polar spot or strip like spot around the star etc.). Here we only try to find location of spots (as an average map) on the surface of the star.

We consider orbital period and epoch which are given by Fekel et al. (2002) to calculate spot longitudes. They give the time of maximum radial velocity as epoch due to zero eccentricity of the orbit and at that time, projection of the apsidal line of the system in perpendicular to observer's line of sight. Here, we subtract one fourth of the orbital period from their epoch by using the advantage of $e = 0$ and calculate longitude values of spots according to the orbital period and modified epoch. In that case, comparing spot locations are easier in terms of longitudes, namely, 0.5 phase corresponds to substellar point (180° longitude) while 0 phase corresponds to its antipode (0° longitude). Then, the resulting elements are

$$T(\mathrm{HJD}) = 2\,449\,292.3621 + 21.^{\mathrm{d}}35957 \times E\,. \qquad (4)$$

Under those assumptions, we run SpotModel code and calculate longitude and angular radius of each individual spot iteratively. Numerical results are given in Table 4. Note that all resulting longitudes are in the reference frame of the binary motion, since the orbital period is used throughout the modelling. We give phased light and color curves, according to the orbital period and modified epoch for every individual subset, together with their theoretical representations in the Appendix (Fig. B1). Since we only used V data for two spot modelling, theoretical color representations in Fig. B1 come from spot temperature modelling of corresponding subset.

In Fig. 8, we show longitudes of two spots versus time. We add 360° to longitude values which are close to 60° for better viewing purpose. Investigation of the plot would be easier if longitude range between 60° and 420° is taken as one 360° rotation of the star. One can notice the existence of two separate spot groups around 180° and 360° longitudes. Filled circles represent spots of Active Longitude 1 (AL1) while open circles show spots of Active Longitude 2 (AL2). AL1 spots are observed between 120° and 240° longitudes while AL2 spots spread between 300° and 420° longitudes, which means, both AL1 and AL2 spots spread over 120° longitude range during 20 years. Another interesting point

Table 4 Numerical results from the two-spot modelling of the 54 individual data sets. φ is the spot longitude, θ is the spot latitude and r is the spot angular radius. Tsp is the spot temperature with its error. AL1 and AL2 denote the active longitudes. Internal errors for Tsp, φ, and r values are given.

			AL1			AL2		
Set No.	Year	Tsp (K)	φ (°)	θ (°)	r (°)	φ (°)	θ (°)	r (°)
1	1992.33	4395±31	217±4	31	21±1	337±5	31	17±1
2	1992.92	4330±97	201±14	44	13±2	329±22	44	9 ±1
3	1993.24	4339±34	197±21	44	9 ±1	340±9	44	12±1
4	1993.41	4359±50	213±7	44	17±1	331±14	44	12±1
5	1993.97	4416±41	210±11	44	15±1	337±6	44	19±1
6	1994.18	4343±25	211±15	44	10±1	347±7	44	16±1
7	1994.34	4280±24	212±10	44	12±1	336±5	44	17±1
8	1994.92	4164±25	237±8	41	18±1	328±6	41	23±1
9	1995.17	4131±13	242±7	41	15±1	335±4	41	21±1
10	1995.38	4140±28	...	...	...	317±1	41	21±1
11	1995.86	4256±50	252±4	35	20±1	88 ±15	35	10±1
12	1996.04	4151±19	238±2	35	23±1	42 ±15	35	8 ±1
13	1996.32	4134±29	233±1	35	31±1	358±4	35	17±1
14	1996.96	4176±51	209±5	33	25±1	329±8	33	18±1
15	1997.11	4022±35	199±3	33	26±1	316±9	33	13±1
16	1997.32	4062±24	189±2	33	29±1	290±4	33	19±1
17	1997.84	4120±29	192±3	26	25±1	299±12	26	12±1
18	1998.04	4280±49	183±2	26	23±1	338±6	26	13±1
19	1998.36	4133±27	157±2	26	25±1	21 ±7	26	12±1
20	1998.93	4301±28	163±3	19	21±1	57 ±3	19	20±1
21	1999.17	4428±33	127±6	19	20±1	29 ±5	19	21±1
22	1999.37	4509±66	101±7	19	22±1	357±6	19	24±1
23	1999.97	4720±43	230±8	31	21±1	350±4	31	34±1
24	2000.16	4731±10	229±8	31	25±1	344±4	31	42±1
25	2000.35	4743±19	216±11	31	22±2	341±4	31	40±1
26	2001.26	4733±129	204±5	5	23±1	332±7	5	21±1
27	2001.40	4742±98	163±5	5	27±1	306±11	5	20±2
28	2002.09	4528±47	131±6	20	25±1	40 ±7	20	22±1
29	2002.24	4441±61	135±10	20	22±1	46 ±9	20	27±2
30	2002.37	4418±49	110±6	20	23±1	15 ±7	20	22±1
31	2003.00	4223±46	106±6	42	18±1	319±10	42	13±1
32	2003.35	4165±21	193±7	42	12±1	75 ±7	42	12±1
33	2003.99	4199±31	193±9	33	16±1	347±11	33	12±1
34	2004.19	4175±44	212±22	33	7 ±1	9 ±5	33	18±1
35	2004.36	4148±25	191±13	33	7 ±1	357±2	33	20±1
36	2004.97	4090±45	197±5	31	16±1	328±4	31	18±1
37	2005.18	4057±27	195±4	31	20±1	317±5	31	17±1
38	2005.37	4024±25	193±4	31	21±1	317±5	31	18±1
39	2005.94	4028±14	159±26	29	5 ±1	31 ±7	29	9 ±1
40	2006.20	4017±32	122±11	29	13±2	210±15	29	10±1
41	2006.36	3992±24	214±5	29	14±1	105±5	29	17±1
42	2006.98	4027±19	210±2	31	24±1	117±6	31	15±1
43	2007.15	4008±36	215±4	31	20±1	116±7	31	15±1
44	2007.37	4011±28	198±8	31	16±2	99 ±15	31	12±1
45	2008.04	4085±24	155±3	36	23±1	34 ±12	36	11±1
46	2008.24	4134±24	176±2	36	22±1	28 ±19	36	7 ±1
47	2008.40	4152±28	175±2	36	24±1	...	...	...
48	2009.08	4258±30	125±8	28	12±1	264±5	28	14±1
49	2009.28	4233±31	181±16	28	10±1	303±9	28	15±1
50	2009.92	4209±45	185±6	28	16±1	67 ±6	28	19±1
51	2010.27	4199±28	179±3	28	22±1	57 ±4	28	21±1
52	2010.90	4263±21	173±3	38	19±1	22 ±18	38	7 ±1
53	2011.11	4323±21	179±4	38	14±1	350±18	38	7 ±1
54	2011.37	4345±40	189±4	38	20±1	317±8	38	14±1

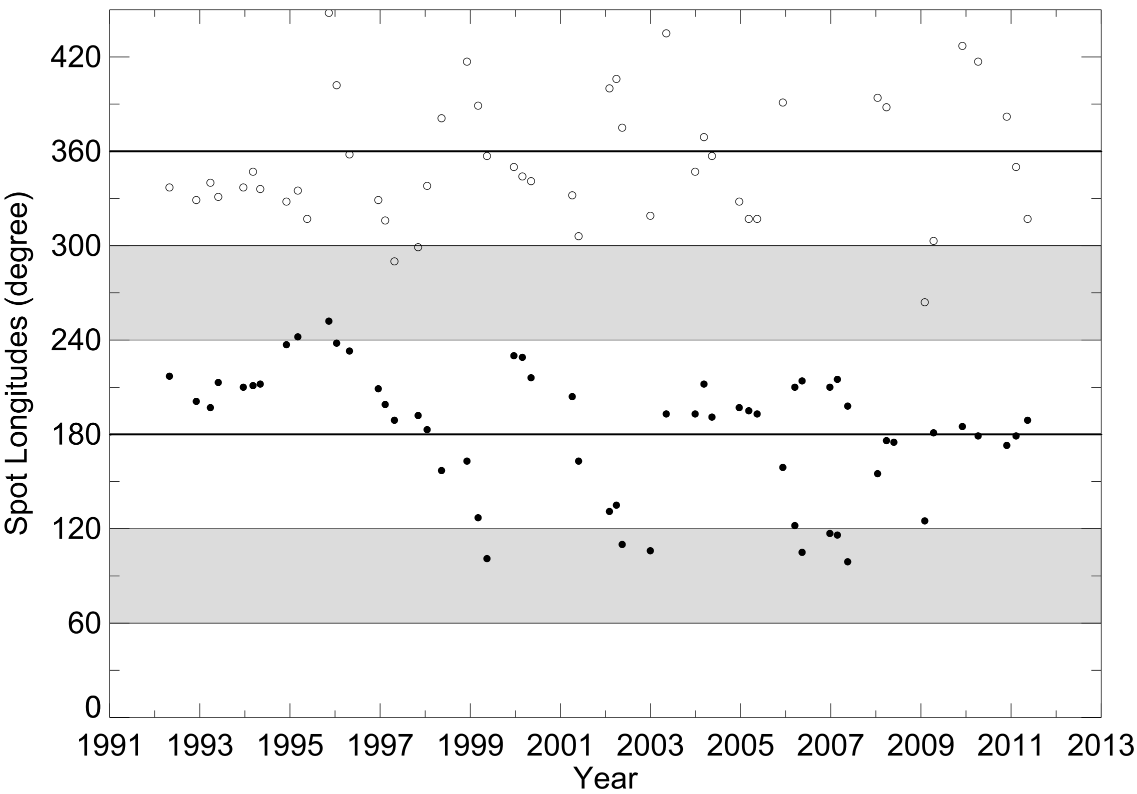

Fig. 8 Longitudinal distribution of spots in time. Two active longitudes, at 180° and 360°, are shown by thick black lines. Filled circles represent AL1 spots, while open circles denote AL2 spots. See the text for explanation of shadowed areas in plot.

is that, for the same time range, there are two 60° longitude ranges which have almost no spot (grey zones in Fig. 8). Those findings are indication of two active and two inactive zones, i.e. active – inactive – active – inactive on the surface of the star. Central longitudes of active zones are 180° and 360°. It means that spots are observed usually around substellar point and opposite to it.

Many parameters determine the spot emerging places on surface of a star. Two main forces in binary systems, which affect spot emerging places, are tidal forces and common magnetic field of the system. Furthermore, for evolved stars, tidal forces are dominant due to smaller gravity of the evolved component. In this case gravitational force of the component star may affect the emerging position of spots. In those kind of systems (UZ Lib, HK Lac, IM Peg, see Oláh 2006a) active longitudes prefer substellar point and opposite side of the star (Oláh 2006a, 2006b). Those results are based on interpretation of observations. Holzwarth & Schüssler (2002, 2003a, 2003b) attempted to investigate the situation in solar type main sequence stars, but calculations have not been broadened to evolved systems except a few attempt (Holzwarth 2004). Here, spot longitude positions on HD 89546 support the observational interpretation of Oláh (2006a). However, different results have been found by Özdarcan et al. (2010) in HD 208472 which is a quite similar system to HD 89546 in terms of absolute and orbital properties. On HD 208472, spots are observed in orbital quadratures instead of substellar point and its antipode. The difference in preferred longitudes of spots among similar systems (i.e. HD 89546, HD 208472, HK Lac) needs to be investigated in theoretical manner in terms of dynamo models.

On the other hand, some interesting motions in spot longitudes are observed over the years for both AL1 and AL2. Until 1996, AL1 and AL2 stay in 60° longitude range inside their individual zones. After 1996 AL1 spots start to move to decreasing longitudes and AL2 spots change their longitude by 120° and start to move towards decreasing longitudes. Result of this motion gives rise to large amplitude and asymmetric (or almost sinusoidal) light curves. Until 2000, AL1 spots keep their motion. From 1998 to 1999, AL2 spots move towards increasing longitudes and this is the only time range when a continuous motion observed towards increasing longitudes. After 1999, AL2 spots move again decreasing longitudes until mid-2001. When AL2 spots on their half way, namely in the beginning of 2001, AL1 spots show sudden change in longitudes by 120° and again move towards decreasing longitudes until mid-2003. While AL1 spots on their half way in mid-2001, AL2 spots show another sudden change in longitude by 120°. This strange sudden change repeat itself for a few times from 1996 to 2006. After 2006 this strange variation pattern disappears and AL1 and AL2 spots get closer in the zone of AL1, until 2009. Towards 2011 AL1 and AL2 spots seem to spread randomly on the star without any clear variation pattern.

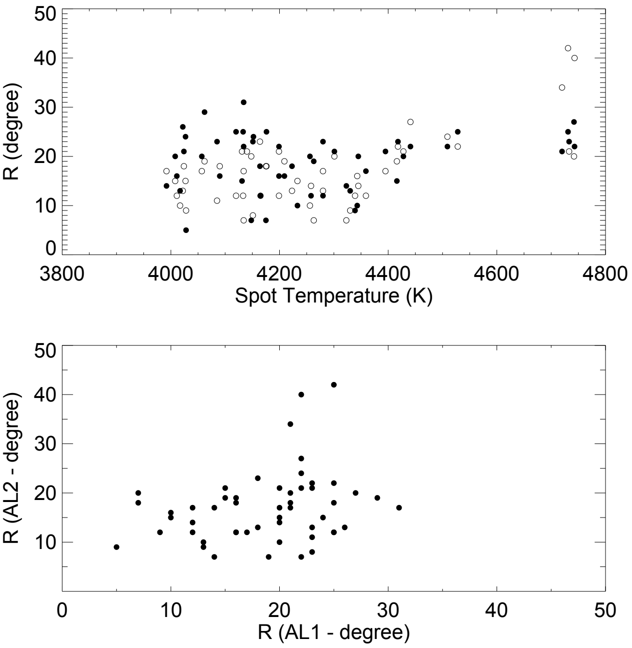

Fig. 9 *Upper panel*: spot temperatures versus angular radii of AL1 spots (filled circles) and AL2 spots (empty circles). *Lower panel*: comparison of angular radii of AL1 and AL2 spots.

Those abrupt changes in spot longitudes looks similar to well known flip-flop phenomenon. In flip-flop phenomenon, main longitude of spot activity changes by 180° in a short time (Jetsu et al. 1991). Here we witness sudden changes in spot longitudes, too, but only by 120° between 1996 and 2007 for both AL1 and AL2.

All those variations in spot longitudes do not seem related to 9-yr cycle which indicate no connection between activity cycle and spot locations in terms of longitudes.This situation is opposite to the observational results of HD 208472 (Özdarcan et al. 2010), although HD 89546 and HD 208472 have quite similar orbital and physical properties. We only observe longitude variations on HD 89546, which originates from the difference between rotational periods and orbital period, because the longitude variations are related to the rotational periods, since for the longitudes (or phases) the orbital period was used.

In Fig. 9 we give a comparison of spot radii and spot temperatures. In the upper panel, we plot angular radii of both AL1 and AL2 spots versus spot temperature. Both for AL1 and AL2 spots, one can observe different angular spot radius for a constant spot temperature which indicates no correlation between spot temperature and spot angular radius. In the lower panel, we compare radii of spots in AL1 and AL2. If we apply a simple linear fit to the distribution, it would give a slope of $\approx$0.30 which means that AL1 spots usually have 30 % larger angular radius than AL2 spots. Since AL1 spots are centered 180° longitude, which corresponds to the place where the giant component faces to unseen component, unseen component may have effects on spot size of AL1 spots, due to the tidal forces.

9 Summary and conclusions

Twenty years of photometric data of HD 89546 show evidence of cyclic activity. The dominant 8.86-yr variation in mean V brightness and variations in photometric period and amplitude in the same time scales suggest a spot activity cycle analog of the solar 11-year sunspot cycle. Further analysis leads us to 22.2-yr longer period variation which might be a cycle like solar Gleissberg cycle. Although its period is longer than the time coverage of current data set, we assume it really exists since we have evidence from orbital period-activity cycle diagram for its existence. Furthermore, we might speculate relations between photometric period-mean brightness and amplitude-photometric period, as observed in the sunspot cycle.

We estimate the differential rotation coefficient, k, by assuming that the photometric period variations mainly come from differential rotation. We use approach of Hall & Busby (1990) for spot latitude range, and our best estimation is $k = 0.086$, which indicates a differential rotation 2 times weaker than the sun. Here we assume that HD 89546 has solar type differential rotation, so the sign of the k is positive. However, it is necessary to obtain high resolution time series spectra and apply Doppler imaging to determine real sign and confirm or refine the magnitude of k.

On the other hand, the distribution of spot longitudes does not show any cyclic variation and seems not related to period, amplitude and brightness variations. There are two active longitudes on HD 89546 (AL1 and AL2) which are spread over 120° longitude range in their zone, while two inactive longitudes, spreading over 60° longitude range, exist between those active longitudes. AL1 is centered around 180° longitudes where the giant star face to unseen companion star, and AL2 is centered around 360° longitude. Therefore, spots are located around substellar point and its antipode on HD 89546. This supports observational interpretation of Oláh (2006a). However, there is not enough theoretical work on emergence location of spots on evolved stars. Further theoretical investigations on evolved stars might shed light on locations and motions of spots in terms of longitude. On the other hand, sudden longitude change of 120° is observed for both AL1 and AL2 spots after 1996 for a few times but that variation pattern is not continuous and disappears towards the end of data set. That event looks like the well known flip-flop phenomenon but its nature seems different.

Acknowledgements. Authors are thankful to Dr. Katalin Oláh for her careful reading and comments which improved the paper. O.Ö. greatly acknowledges supports from the Turkish Scientific and Technical Research Council TÜBİTAK and Ege University Science Fund, under Project No. 2008/Fen/061. This study has made use of the SIMBAD database, operated at CDS, Strasbourg, France. GWH acknowledges long-term support from NASA, NSF, Tennessee State University, and the State of Tennessee through their Centers of Excellence Program.

References

Budding, E.: 1977, Ap&SS 48, 207
Drilling, J.S., Landolt, A.U.: 2000, in: A.N. Cox (ed.), *Allens Astrophysical Quantities*, p. 388
Fekel, F.C., Henry, G.W., Eaton, J.A., Sperauskas, J., Hall, D.S.: 2002, AJ 124, 1064
Flower, P.J.: 1996, ApJ 469, 355
Gray, D.F.: 2005, *The Observation and Analysis of Stellar Photospheres*, 3rd ed., Cambridge Univ. Press
Hall, D.S., Busby, M.R.: 1990, in: C. Ibanoglu (ed.), *Active Close Binaries*, p. 377
Hathaway, D.H., Wilson, R.M.: 1990, ApJ 357, 271
Henry, G.W.: 1995, in: G.W. Henry, J.A. Eaton (eds.), *Robotic Telescopes. Current Capabilities, Present Developments, and Future Prospects for Automated Astronomy*, ASPC 79, p. 44
Henry, G.W., Fekel, F.C., Hall, D.S.: 1995, AJ 110, 2926
Holzwarth, V.: 2004, AN 325, 408
Holzwarth, V., Schüssler, M.: 2002, AN 323, 399
Holzwarth, V., Schüssler, M.: 2003a, A&A 405, 291
Holzwarth, V., Schüssler, M.: 2003b, A&A 405, 303
Jetsu, L., Pelt, J., Tuominen, I., Nations, H.: 1991, LNP 380, 381
Lenz, P., Breger, M.: 2005, Communications in Asteroseismology 146, 53
Levenberg, K.: 1944, Quart. Appl. Math. 2, 164
Marino, G., Catalano, S., Frasca, A., Marilli, E., Teriaca, L.: 2002, IVBS 5227, 1
Marquardt, D.W.: 1963, SIAM J. Appl. Math. 11, 431
Montes, D., Fernández-Figueroa, M. J., De Castro, E., Cornide, M., Latorre, A., Sanz-Forcada,J.: 2000, A&AS 146, 103
Oláh, K.: 2006a, Ap&SS 304, 145
Oláh, K.: 2006b, in: W.I. Hartkopf, E.F. Guinan, P. Harmanec (eds.), *The Influence of Binarity on Stellar Activity*, p. 442
Oláh, K., Strassmeier, K.G.: 2002, AN 323, 361
Oláh, K., Kövari, Zs., Bartus, J., Strassmeier, K.G., Hall, D. S., Henry, G. W.: 1997, A&A 321, 811
Özdarcan, O., Evren, S., Strassmeier, K.G., Granzer, T., Henry, G.W.: 2010, AN 331, 794
Pulkkinen, P., Tuominen, I.: 1998, A&A 332, 748
Ribárik, G., Oláh, K., Strassmeier, K.G.: 2003, AN 324, 202
Schwarzenberg-Czerny, A.: 1989, MNRAS 241, 153
Strassmeier, K.G.: 1994, A&AS 103, 413
Strassmeier, K.G., Handler, G., Paunzen, E., Rauth, M.: 1994, A&A 281, 855
van Hamme, W.: 1993, AJ 106, 2096
van Leeuwen, F.: 2007, A&A 474, 653
Vanmunster, A.: 2007, http://www.peranso.com/

A Transformation coefficients for the EUO photometric data

Equations (A1) and (A2) are for 27 March 2009 and 17 April 2009, respectively. Errors for the last two digits of each coefficient are given parentheses.

$$\begin{aligned} V - v_0 &= -0.090(28) \times (B - V) + 18.726(17), \\ B - V &= 1.133(36) \times (b - v)_0 - 0.457(11), \end{aligned} \tag{A1}$$

$$\begin{aligned} V - v_0 &= -0.068(43) \times (B - V) + 18.791(24), \\ B - V &= 1.118(18) \times (b - v)_0 - 0.441(05). \end{aligned} \tag{A2}$$

B Phased light curves for 54 data sets and their spot model representations

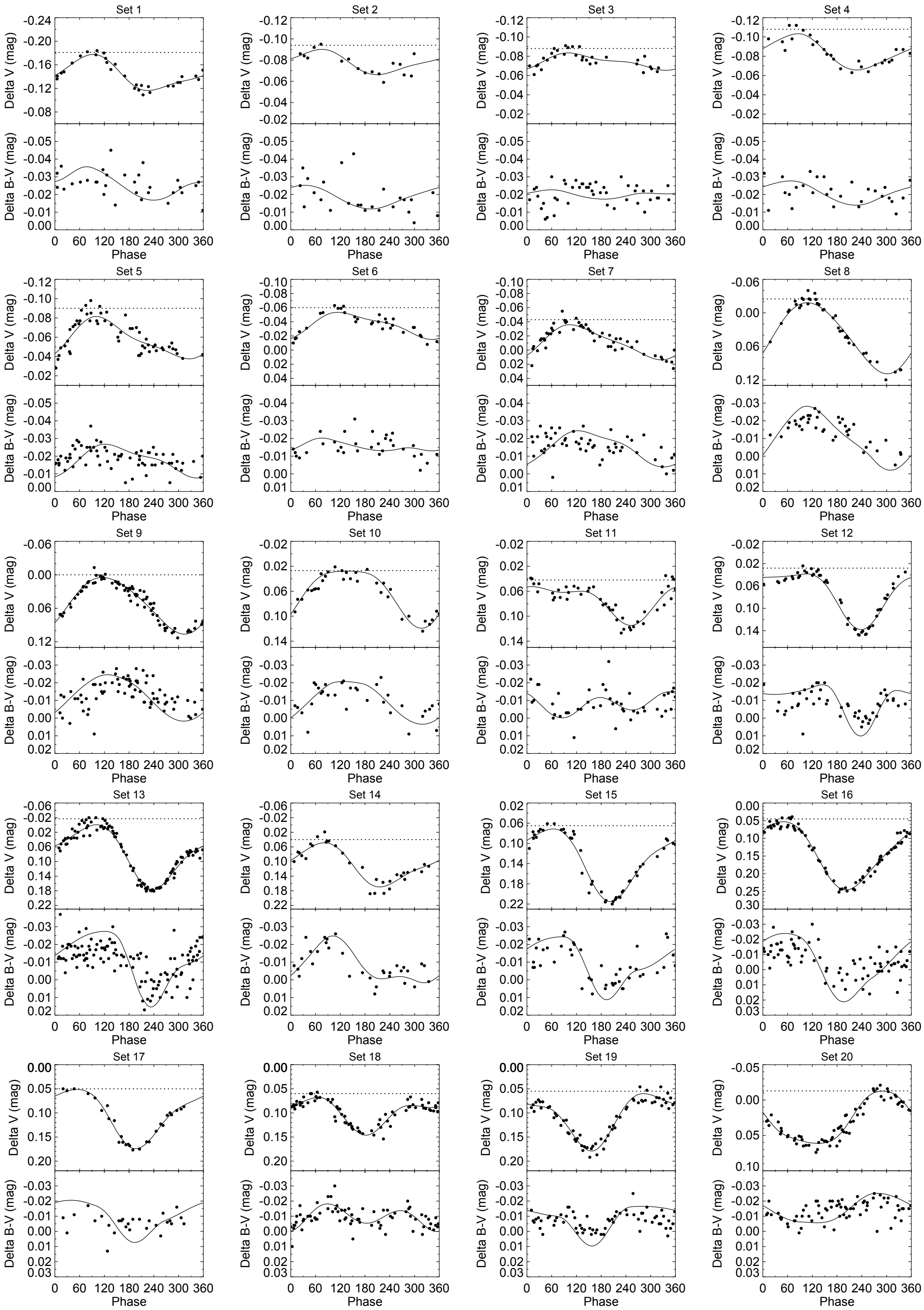

Fig. B1 Light and color curves of the 54 individual data sets (filled circles), phased (in degrees) to the orbital period. Data set numbers from Table 4 are used as plot titles. Horizontal dashed lines show maximum light level in each set while the continuous curves represent the corresponding spot model. Note that color representations come from spot temperature modelling.

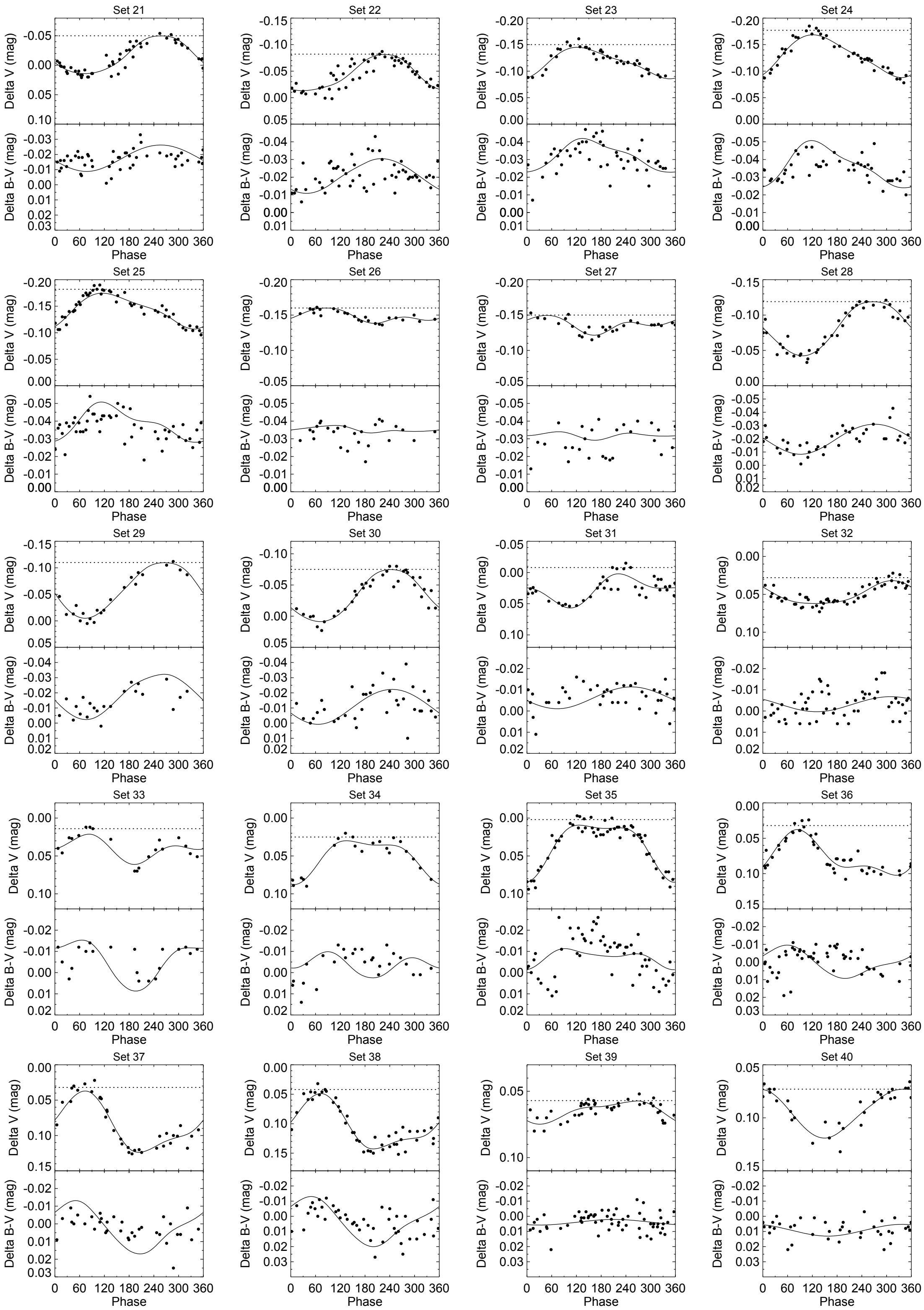

Fig. B1 Continued.

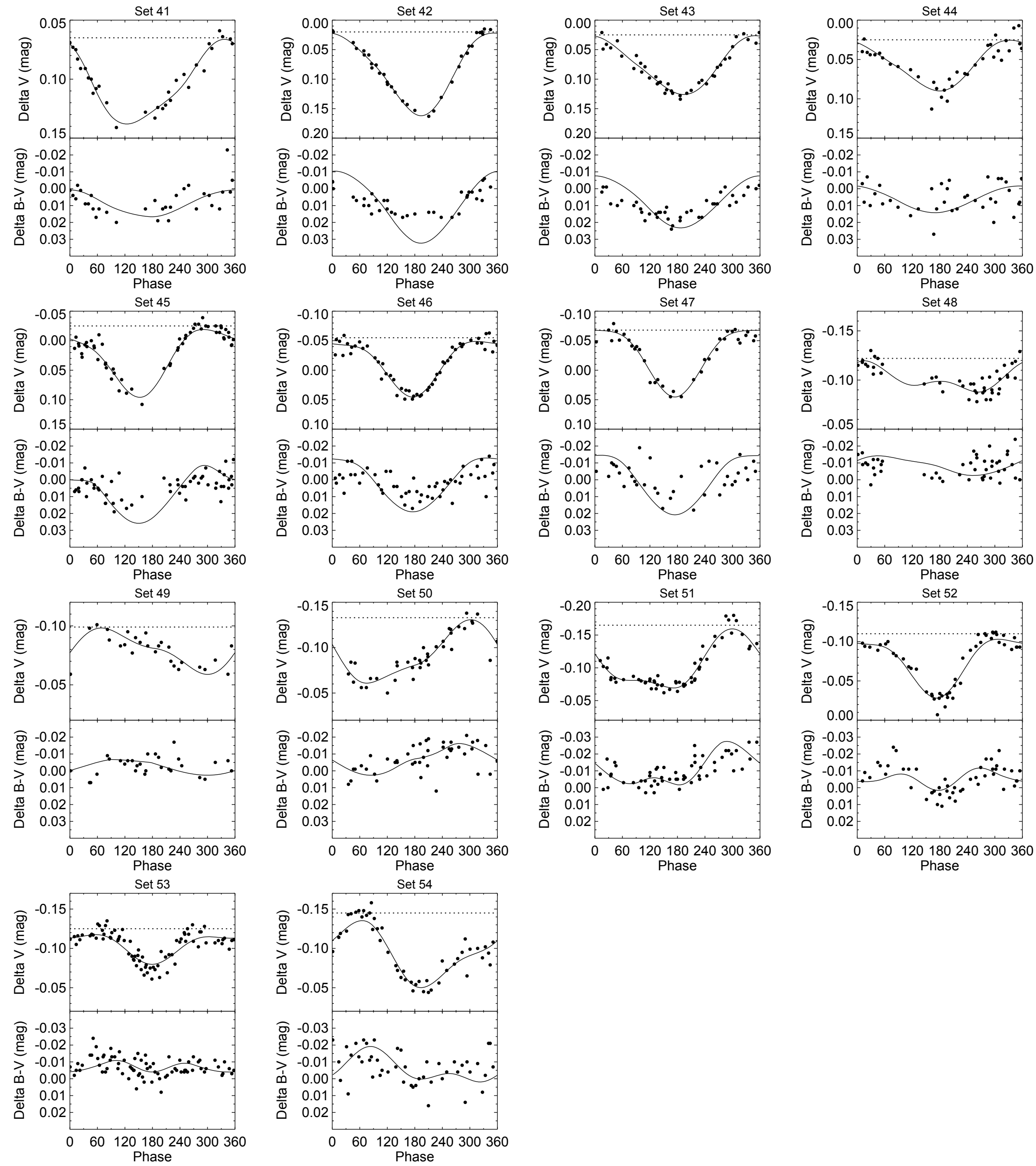

Fig. B1 Continued.